

Identification of non-idealities in gel electrophoresis

Christina M. Bondy, David W. Siitari, Thatcher W. Root, Edwin N. Lightfoot*

University of Wisconsin–Madison, Department of Chemical and Biological Engineering, 1415 Engineering Drive, Madison, WI 53706, USA

Available online 25 May 2005

Abstract

The molecular weight separation, which is the second dimension of two-dimensional gel electrophoresis, is studied quantitatively with the goal of improving positional predictability and reproducibility. Mathematical modeling of carrier electrolyte dynamics is used to track the progress of a stacking front as a function of coulombs passed. In all test cases, the front moves more slowly than predicted and shows both curvature and tilt. These systematic deviations from the model are found to be influenced by a variety of factors, including both design and operating features. These factors are largely explained, and suggestions are made for improvements.

© 2005 Published by Elsevier B.V.

Keywords: Electrophoresis; Reproducibility; Modeling; Proteomics; SDS-PAGE

1. Introduction

Two-dimensional gel electrophoresis was developed in 1975 to obtain high resolution, highly sensitive separations of protein mixtures [1]. It has become a widely used tool for proteomics because of its ability to separate large numbers of proteins. The use of two orthogonal separations, isoelectric focusing and sodium dodecyl sulfate-polyacrylamide gel electrophoresis (SDS-PAGE), allows the technique to be used for many classes of proteins. Further, it can be used to detect changes in protein regulation in response to the cell environment. However, while it is a valuable tool for separating complex protein mixtures, its utility is often limited by lack of quantitative reproducibility [2,3]. In fact, replicate runs of the same sample can have a standard deviation in spot position of the same order of magnitude as the distance between protein spots from complex mixtures.

Presented here is a preliminary dynamic model intended to capture the essence of carrier electrolyte migration. This in turn provides the basis for protein migration and is needed to begin a serious study of the second stage of two-dimensional gel electrophoresis. Pared to its essentials, this process can be described as a continuing one-dimensional replacement of the chloride anions originally present in the gels by glycinate

ions from the upper reservoir of the apparatus. The system is sufficiently complex that investigation must begin with a model faithful enough to describe its characteristic behavior but simple enough to provide useful insight to the investigator. In this investigation such a model must describe migration of complex ionic mixtures in an electric field in the presence of equilibrium partial dissociation of glycine and Tris base.

The model is used to follow the progress of a tracer dye through the gel matrix. The electrolyte anions are present under the proper conditions to form a stacking front, which occurs when an ion of high mobility is replaced by one of lower mobility [4–6]. The first ion has a tendency to move faster and run away from the second, but this would produce a region of no ions and thus no current, which cannot occur. As a result, the two ions travel at the same velocity and a sharp interface forms between them. If an ion of intermediate mobility is added to the system, it will travel with this interface. Since chloride is more mobile than glycinate, a stacking front forms. The dye bromophenol blue has an intermediate mobility. Thus, it moves with the stacking front, allowing the progress of the separation to be tracked. Both the anion concentration and the voltage gradient change dramatically across this interface. The proteins, which are inhibited by the gel matrix, travel behind the dye front in the glycinate portion of the gel. Fig. 1 shows this configuration schematically.

Also presented are a large variety of experimental data in which electrolyte composition, operating conditions and

* Corresponding author. Tel.: +1 608 2632018; fax: +1 608 262 5434.
E-mail address: enlightf@wisc.edu (E.N. Lightfoot).

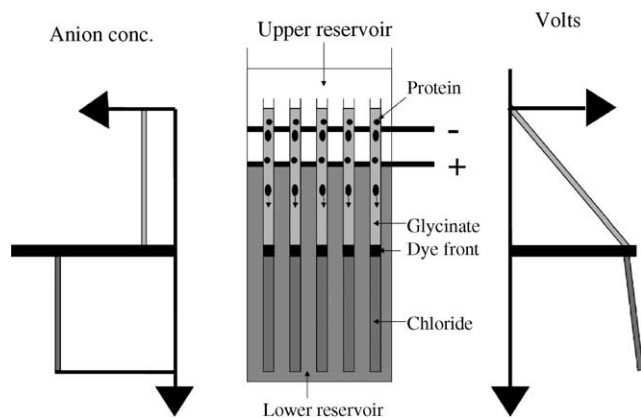


Fig. 1. Schematic representation of the experimental apparatus. This side view shows the positions of the five gels as well as the upper and lower reservoir buffers. The chloride and glycinate regions and the dye front are indicated and proteins are shown. The schematic omits the representation of the pump that circulates the cooling buffer through the system. On the left, the anion concentration in each zone of the gel is represented, and on the right is the voltage gradient in each part of the gel.

equipment configuration are varied systematically. The model shows encouraging agreement with the data, but significant deviations from the model prediction are observed under all conditions tested. Critical comparisons between prediction and observation have proven useful for identifying significant non-idealities and have led to suggestions for changing both operating conditions and equipment design.

2. Experimental

2.1. Basic equipment

Electrophoresis was performed using the Genomic Solutions Investigator system. This apparatus, shown schematically in the center panel of Fig. 1, contains five gel plates in parallel; each approximately 20 cm \times 24 cm \times 1 mm sheet of polyacrylamide was cast between \sim 3 mm thick glass plates. The matrix was 10% Duracryl (Genomic Solutions, Ann Arbor MI) with 2.2% crosslinking. The gel buffer was 315 mM tris(hydroxymethyl)aminomethane (Tris base) with 123 mM Tris-HCl, pH 8.9. When sodium dodecyl sulfate (SDS) was used, it was at a concentration of 3.7 mM. The buffer temperature during the run ranged from 5 to 13 $^{\circ}$ C, but was usually \sim 6 $^{\circ}$ C. Gels were run at a constant power of 16 W/gel. Not shown in the figure is a centrifugal pump, mounted at the base of the apparatus to provide mixing, and hence cooling, of the lower buffer.

The reservoir buffers were mixtures of partially dissociated Tris and glycine. The upper buffer was 50 mM Tris base with 384 mM glycine, pH \sim 8.3. When SDS was used it was at a concentration of 6.9 mM. The bottom buffer had the same solute proportions as the top but was diluted 1:1 with 18 M Ω water. Buffer concentrations were altered for some experiments, as described.

The presence of the chloride and glycinate regions as well as an intermediate sodium dodecyl sulfate region was found using silver chloride precipitation. To detect these zones, a gel was run for 2.5 h, until the dye front was \sim 9 cm from the bottom of the gel. Then, the gel was removed from the glass plates and placed in a 7.8 mM solution of silver nitrate. Silver chloride forms a white precipitate, so the location of the chloride was detectable by looking at the gel.

Most experiments in this study followed the progress of the dye front with no proteins present. However, to track the progress of proteins and determine their correlation to dye front migration, Bio-Rad's Kaleidoscope standards were used (Bio-Rad Laboratories, Hercules CA). For these experiments, a gel was cast with a 15-well comb. Thirty microliters of the standard were added to four of the wells, with the filled positions varying from run to run.

2.2. Equipment modifications

In specified experiments, apparatus modifications were made to alter the ion paths through the gel. The parts of the electrodes that extended horizontally beyond the edges of the gels were masked (with electrician's tape) so that no current was generated beyond the edges of the gels. To a similar end, the top buffer chamber was blocked beyond the edges of the gels. Specially designed polyvinylchloride blocks were made to fit over the ends of the glass plates where the spacers are located. They filled up the region that would otherwise be filled with buffer so that the current paths did not extend beyond the edges of the gels. For another approach to produce uniform current paths, auxiliary electrodes were used: copper wire was attached to the top and bottom of the glass plates on one of the gels. For the auxiliary electrode experiments, two gels were run, one with the extra electrodes and one without them.

Modifications were also implemented to improve mixing and thus cooling of the lower buffer. Two different configurations were used for the rack that held the gels. The original rack provided with the box had four slits in each of its side panels, one between each pair of gels, to allow the circulating buffer to flow between the gels. However, flow is disturbed because the 1 cm wide slits are narrower than the 2.3 cm spaces between the gels. A newly designed gel rack had a honeycomb pattern of holes to allow less restricted flow of the cooling buffer between the gels and to act as a guide to ensure more nearly uniform flow.

2.3. Procedures

For the modifications described above, as well as the unmodified box, the ion migration was analyzed on the basis of the shape of the dye front as it moved through the gel. The width of the gel was approximately 24 cm. The distance from the bottom of the gel to the dye front was measured at transverse positions of 4, 8, 12, 16, and 20 cm at 30 min intervals for fitting and characterization of stacking front skew and curvature.

Stirring in the lower buffer reservoir was diagnosed by observing the mixing of dye or the trajectories of oil drops in the gel box. Bromophenol blue was injected between the gels in the first and second slots and pictures were taken at regular intervals. This gave a qualitative picture of the mixing in the box. More quantitative information was gained by injecting neutrally buoyant oil drops. A mixture of ~84% dibutyl phthalate and 16% heptane with a small amount of the dye methyl red was injected in drops between the gels in the first and second slots. Pictures were taken every 15 s. The paths of the oil drops could be determined and the velocity of the drops could be calculated.

3. Background and assumptions

Before the model is developed, several preliminary details must be addressed. First, parameters necessary for calculations based on the model must be found. A combination of literature values and experimental measurements are used, as presented in Appendix A. Second, assumptions and approximations used in model development must be identified.

In the applied field, the anions move down through the gel and form a stacking front, which results from the lower mobility of glycinate relative to chloride (see Fig. 1). The bromophenol blue tracer dye, which has a mobility intermediate between glycinate and chloride, is stacked between these two anions.

The separation is thus tracked by this dye, which is normally loaded along with the proteins. Since the carrier electrolytes are at a much higher concentration than the proteins, the protein contributions to current can be neglected. Therefore, the model describes the velocity of carrier electrolytes in the gel in the absence of proteins. The model is compared to experimental data by tracking the movement of the tracer dye during the separation. The presence of proteins in the gel was shown in preliminary experiments not to affect the dye tracer movement significantly, confirming the assumption that protein contributions to overall conductivity can be neglected.

It is preferable to begin with the simplest realistic test system and to simplify the transport picture as far as possible using order-of-magnitude arguments. Simplification of the transport mechanisms is made possible by considering the time scales and the influence of solution composition characteristics on the migration process. Here, the following simplifications are adopted:

- (1) Electroneutrality is valid throughout the system.
- (2) Concentration diffusion is much slower than electrodiffusion and will be neglected. This means that undissociated glycine and Tris are immobile.
- (3) Solution concentrations are low enough that ion–ion diffusional interactions are of only secondary importance, and they will also be neglected.
- (4) Relative mobilities of the ions are constant.

- (5) The current lines are perpendicular to the top of the gel, and the current density is uniform.

Approximation (1) is a well-established phenomenon. Electroneutrality states that the sum of the charges in any local area is zero. In this case, with single charges on each electrolyte, this means that the anion concentration is equal to the cation concentration in each section of the system. In practice, concentrations typically differ on the order of 10^{-13} M [7], making this a very good approximation.

Approximation (2) depends on the relative magnitudes of concentration diffusion and electrochemical migration. The penetration distance ([8], Eq. (12.1–12.9)) is given by

$$\delta = 4\sqrt{Dt} \quad (1)$$

For a typical electrophoresis separation of 6 h, given a diffusion coefficient for Tris and glycine of $\sim 1 \times 10^{-5}$ cm²/s, the penetration distance is approximately 1.9 cm, which is an order of magnitude lower than the distance the dye travels over that time. Therefore, concentration diffusion is much slower than migration and can be neglected. In fact, the sharp band of dye tracer provides direct evidence that concentration diffusion is negligible and that there is a sharp interface between the chloride and glycinate portions of the gel.

Approximations (3) and (4) allow neglect of several unknown contributions to ion mobilities. The neglect of ion–ion diffusional reactions is necessary to obtain a tractable description, and it has been found acceptable by the vast majority of electrochemists working with such dilute solutions. Using constant relative mobilities eliminates the unknown effects of temperature.

Approximation (5) is the idealization used implicitly in essentially all two-dimensional gel electrophoresis procedures. It provides the geometric basis from which departures due to equipment geometry can be determined.

4. Model development

Now that the basic theory has been introduced, parameters determined and assumptions presented, a dynamic model predicting the distance traveled by the tracer dye as a function of time can be developed. The complications presented by the presence of SDS in the gel were neglected in this preliminary model. Therefore, the model is for a system that has only Tris glycinate in the upper and lower buffers and Tris chloride in the gel. As time progresses, the glycinate from the upper buffer replaces the chloride in the gel, and Tris migrates upward through the gel from the lower buffer. The model attempts to describe this ion migration by using a combination of mass transport, thermodynamics, and electrochemistry with no adjustable parameters.

Using the current through the gel as a basis, the distance traveled by the stacking front can be related to the coulombs passed, thus eliminating time from the description. The current is continuous throughout the system; therefore, the

measured value can be used directly. This eliminates the need to estimate the reservoir contribution to the voltage drop. Additionally, it is not necessary to calculate all of the ion concentrations since only the chloride concentration is needed. Further, since the conductances only appear as ratios, their actual values and temperature dependences are less important than if they stood alone. The expression for current as a function of velocity is shown in Eqs. (B.1) and (B.2) in Appendix B. More specifically for our system:

$$\begin{aligned} I &= AF(c_{\text{Cl}^-}v_{\text{Cl}^-} - c_{\text{T}^+, \text{L}}v_{\text{T}^+, \text{L}}) \\ &= AF(c_{\text{G}^-}v_{\text{G}^-} - c_{\text{T}^+, \text{U}}v_{\text{T}^+, \text{U}}) \end{aligned} \quad (2)$$

where I is the current, A is the cross-sectional area, F is Faraday's constant, c_i is concentration and v_i is velocity. The subscripts are defined as follows: Cl^- chloride; T^+, L Tris in the lower part of the gel; G^- glycinate; and T^+, U Tris in the upper portion of the gel.

The expression above can be manipulated, as shown in Appendix B, to give a relationship between the velocity of the chloride/glycinate interface and the current in the gel.

$$v_{\text{interface}} = \frac{I}{AFc_{\text{Cl}^-}(1 + (\lambda_{\text{T}^+, \text{L}}/\lambda_{\text{Cl}^-}))} \quad (3)$$

The velocity of the stacking front is given by $v_{\text{interface}}$, and the λ 's represent the equivalent conductances of the ions. Integrating with respect to time will give a relationship between distance traveled and coulombs passed. Q is the number of coulombs passed through the system when the dye front has traveled a distance x .

$$x = \frac{Q}{AFc_{\text{Cl}^-}(1 + (\lambda_{\text{T}^+, \text{L}}/\lambda_{\text{Cl}^-}))} \quad (4)$$

Now these predictions are used to probe the behavior of the equipment provided by the manufacturer. Some unexpected behavior is found which suggests problems both with operating conditions and with the apparatus itself. Then the apparatus is modified to test these suggestions and it is found that improved operation can result.

5. Preliminary study of the unmodified equipment

The initial experimental work described immediately below is basically a critical comparison between actual operation and the predictions of Eq. (4), and the following discussion consists of attempts to identify the causes of discrepancies between observation and prediction.

5.1. Comparison of prediction and observation

The relationship between distance traveled by the stacking front and coulombs passed through the gel for the model prediction (Eq. (4)) was compared to a variety of experimental conditions. The model predicts a linear relationship between

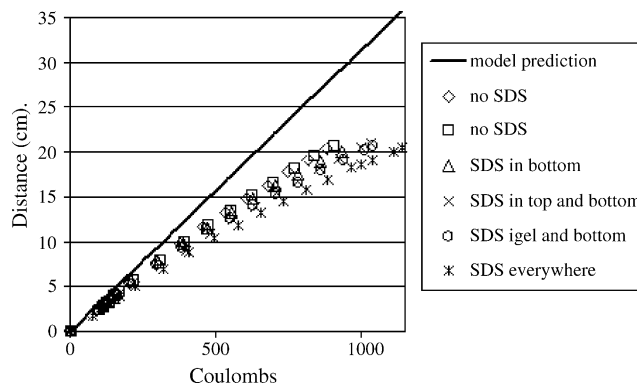


Fig. 2. Effects of SDS on coulomb efficiency. Gels with no SDS are closest to the model predictions. As SDS was added to more parts of the system, the results deviated further from the model.

coulombs and distance. On the other hand, all of the experimental data sets, for a wide range of conditions, curve away from the model prediction (some representations of this behavior can be seen in Figs. 2–4). Closer examination of data shows the best agreement between the model prediction and the experimental results are found for runs in which SDS is omitted from all buffers (see for example Fig. 2). However, as shown in Figs. 3 and 4, the compositions of the upper and lower buffers also have appreciable effects. These effects will be discussed in the following section.

First however, it is noted that substantial discrepancies between observation and prediction always occur, even in the absence of SDS or for fresh and standard buffers in all three regions. Moreover, the shapes of observed and predicted curves are different. The pronounced curvature in all observations cannot be ascribed to errors in electrolyte mobilities. Rather the straight line of the prediction, indicating a constant coulomb transport efficiency, is an inherent consequence of the stacking front concept.

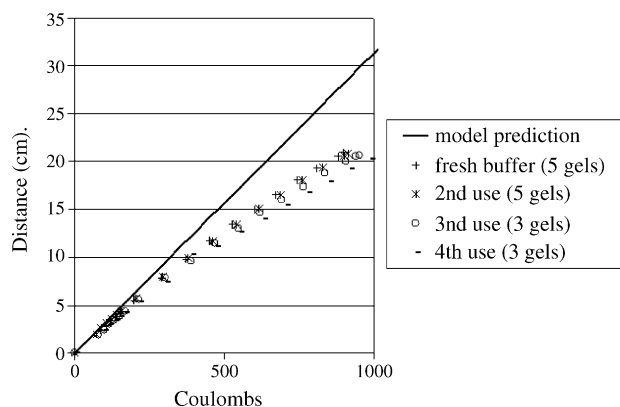


Fig. 3. Effects of reuse of the bottom buffer. The same buffer was recycled for all four runs. The fresh buffer results were closest to the model. No noticeable change occurred for the second set of gels run, but the efficiency got progressively worse after that. No protein was run in these experiments and SDS was omitted from all gels and buffers.

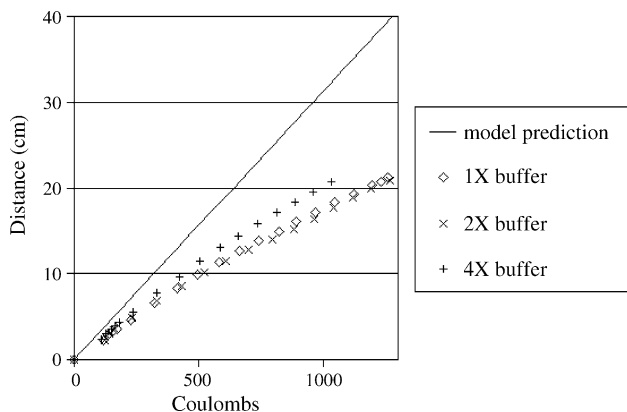


Fig. 4. Effects of top buffer concentration on coulomb efficiency. All gels and buffers contained SDS. The 2× buffer is the usual concentration in the top buffer. The 1× experiment was the second use of the bottom buffer, the 2× was the third, and the 4× was the fourth. The efficiency increased for the 4× buffer despite the recycled bottom buffer. One gel was run in each of the four experiments using the same bottom buffer.

Direct evidence of departures from the one-dimensional transport postulated above is shown in Fig. 5. Here identical mixtures of prestained proteins (Kaleidoscope standards, Bio-Rad) were run in four lanes. Vertical guide lines are superimposed on the figure to assist with detection of the divergence of the proteins from vertical migration. The curved line at the bottom of the gel is the dye front, which is approximately perpendicular to a line through proteins from the same lane. In typical runs, curvature of the dye front, referred to as a “smile,” and significant tilt from the horizontal are observed. There is significant run-to-run variation as shall be seen in more detail later. It becomes clear now that at least

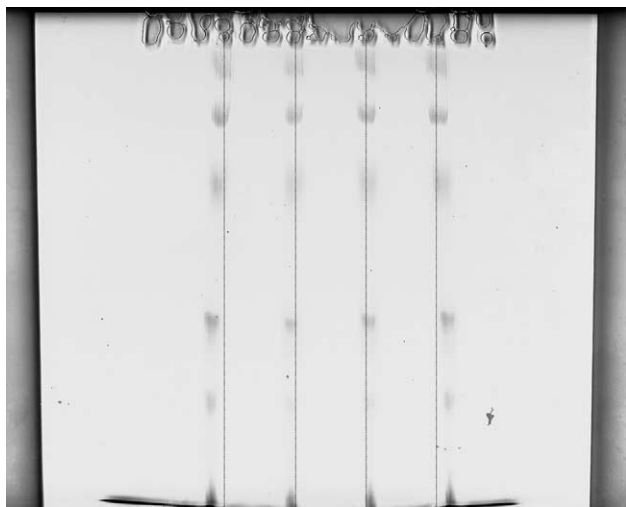


Fig. 5. Scan of a gel in which 30 μ L of Bio-Rad Kaleidoscope standard was run in each of lanes 4, 7, 10, and 13. The protein spots can be seen in each lane. The heavy line at the bottom, which is not entirely visible, is the dye front. The superimposed dashed lines in each lane indicate the path perpendicular to the top of the gel. Protein paths can be seen to diverge from this line toward the nearest edge of the gel.

some of the curvature in observed stacking fronts is due to departures from the postulated one-dimensional migration.

5.2. Discussion

It is now clear that there are two kinds of departures from predicted behavior, one resulting from buffer compositions and another from equipment characteristics. We now look at these in turn, and we begin with the composition-dependent effects.

5.2.1. Sodium dodecyl sulfate effects

The effect of SDS is the largest, and it is suggested in Fig. 6 that it results from the formation of a third zone between the dye front and the chloride zone. Shown in Fig. 6 is the result of washing a gel, after removal of the glass plates, in aqueous silver nitrate. The clouded region at the bottom of the figure is due to a precipitate of silver chloride, and it clearly shows that the chloride zone does not extend to the dye front. This intermediate zone is occupied by the DS anion, which is more mobile than either glycinate or the dye, but less mobile than chloride. Search of the prior literature [9] confirmed this statement: Using 35 S-labeled SDS showed the accumulation of sodium dodecyl sulfate in this intermediate region.

5.2.2. Buffer concentration effects

Other important contributing factors to the ion migration in the gel are the buffer concentrations in the upper and lower reservoirs, as shown in Figs. 3 and 4. Fig. 3 shows the relationship between distance traveled by the stacking front and coulombs passed through the gel for various concentrations and compositions of the bottom buffer. The composition changes as chloride runs into the bottom buffer from the gels

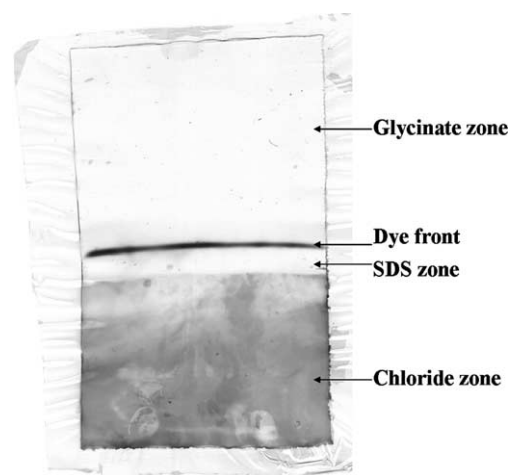


Fig. 6. A partially run gel after immersion in silver nitrate solution. The lower part of the gel contains chloride, which forms a white precipitate with silver. A sharp interface marks the beginning of the stacking zone, seen as a refractive index change in the unstained gel. The dye marks the trailing edge of the stacking zone. In gels with SDS, the stacking zone is broad because of the accumulation of SDS behind the interface.

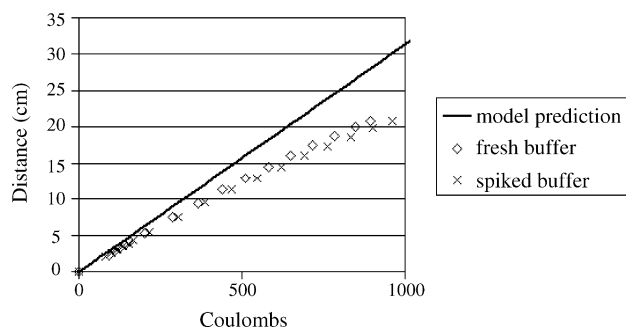


Fig. 7. Effects of chloride on the coulomb efficiency. Fresh bottom buffer was used in the first run. Seven milliliters of HCl were added to the lower buffer between the first and second runs. There was no SDS in the gels or the buffers, and no proteins were run. Three gels were run in each experiment.

and the 2.5 L upper reservoir containing 2× buffer is emptied into the original 1× buffer between runs. The concentration of the bottom buffer increases with each run, and as it does the deviation grows between the model prediction and the experimental result. The standard operating procedures that accompanied the equipment suggests that the buffer can be recycled up to three times. Both in practice and in the model, it is assumed that the reservoirs do not affect the outcome of the separation in any way. They are treated as infinite sources and sinks for ions. However, observations indicate that the buffer composition influences the extent of the deviation from the predicted velocity, with the deviation growing as the lower buffer concentration increases.

5.2.3. Chloride effects

Preliminary observations indicated that the amount of chloride in the bottom buffer, rather than the Tris and glycine concentrations, was primarily responsible for the increased deviations from model predictions. When fewer gels were run in early experiments, it took more runs for deviations to be noticeable. To test this hypothesis, the bottom buffer was spiked with 7 mL of hydrochloric acid (about 15 gels-worth of chloride anions) between the first and second runs. Fig. 7 shows the relationship between distance traveled by the stacking front and coulombs passed through the gel for fresh bottom buffer and bottom buffer spiked with chloride. Comparing these results with the results in Fig. 3, it can be noted that adding chloride ions increased the deviation between the first and second runs compared to the deviation caused by the concentration change in normal operation. In previous experiments, significant deviations from the fresh buffer results were never noticeable before the third run. Typically, at least seven gels were run before a deviation was observed. This confirmed the hypothesis that adding chloride to the bottom buffer was at least in part responsible for the differences between the results for gels with fresh buffer and those with recycled buffer. It also points to the fact that the buffers are not effectively infinite sources and sinks for ions. Cations in the bottom buffer migrate up through the gel; thus, they are expected to play a role in the current efficiency in

the gel. Anions in the bottom, however, are not expected to directly contribute to migration in the gel. The importance of the chloride concentration in the bottom buffer suggests that the reservoir has an important, and as of now not fully understood, influence on ion migration.

5.2.4. Remaining effects

Since the bottom buffer had a significant effect on ion migration, it was expected that the top buffer concentration would also be important. As anticipated, the top buffer concentration influenced the size of the difference between the model and the experimental results. Fig. 4 shows the relationship between distance traveled by the stacking front and coulombs passed through the gel for several concentrations of the top buffer. The usual top buffer concentration of 2× and a 1:1 dilution of that buffer show similar results. A 4× buffer, however, was significantly closer to the model prediction than the less concentrated buffers. In general, the top buffer is replaced, so its concentration is the same for every run. Therefore, sensitivity to its concentration is not as important a consideration for reproducibility as is the concentration of the bottom buffer.

The remaining deviations require further investigation, but two general classes of suspects appear likely. The first is basic geometry of the electrodes and buffer chambers. The second is thermal inequality resulting from insufficient cooling, which can result from insufficient pumping as well as lower buffer chamber geometry. Both can produce curvature of the current lines and lower than expected coulomb efficiency. Both of these possibilities were investigated as indicated immediately below, and in both cases the non-idealities were described by fitting the observed dye fronts to a simple second order equation:

$$Y = C_0 + C_1 X + C_2 X^2 \quad (5)$$

where Y is the vertical position of the dye front measured downwards, X the corresponding horizontal position measured from the centerline, and C_0 the vertical position of the dye front at the center of the gel. The coefficients C_1 and C_2 were used to characterize the skewing and curvature of the dye front, respectively, and to monitor how these properties varied as a function of distance traveled by the center of the dye front (12 cm measurement). Note that a positive value of C_1 shows a tilt downward to the right, and a positive value of C_2 shows a “frown”. Ideally both the coefficients C_1 and C_2 would be zero, indicating that the dye front is straight and horizontal throughout the trajectory.

6. Equipment modifications

6.1. Electrode geometry and field distributions

Our first approach to identifying geometric non-idealities was to mask the ends of the electrodes and to block the regions

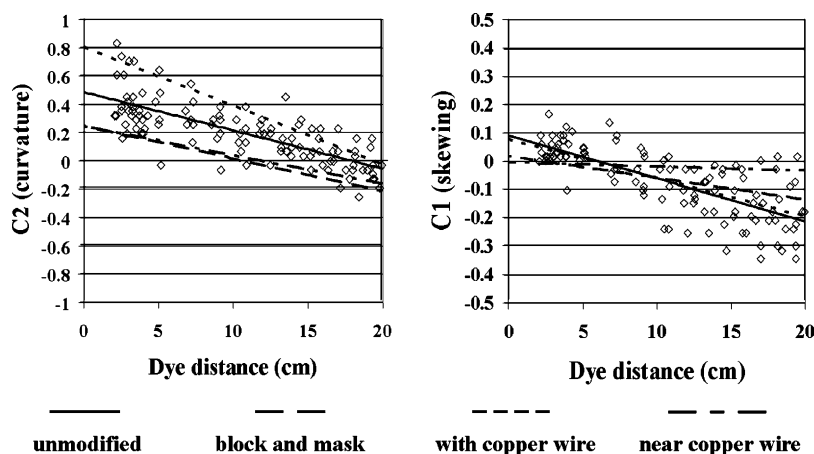


Fig. 8. Curvature and skewing of dye fronts run in the unmodified box, a box with masked electrodes and blocked buffer, and a box with masked electrodes and blocked buffer for gels with auxiliary electrodes and those run next to gels with auxiliary electrodes.

of the upper buffer reservoir that extend horizontally beyond the edges of the gels. The left panel of Fig. 8 describes the curvature of the dye front as a function of mean distance traveled. In both the modified and the unmodified boxes, the curvature begins as a “frown” and changes to a “smile”. However, the magnitude of curvature is significantly less with blocking and masking than it is in the unmodified box. The skewing or tilt, described by C_1 and shown in the right panel of Fig. 8, is also less. In addition, the points on these plots show the data for the unmodified box, which has the maximum observed scatter. Other points are omitted in order to simplify the plots, but the scatter of the data for repeated runs is reduced in the blocked and masked box compared to the data for the unmodified box.

Also shown in Fig. 8 are the curvature and skewing for auxiliary electrodes on one gel. These auxiliary electrodes are simple copper wires fixed horizontally to hold local voltages more nearly constant over their lengths. Separate results are shown for the gel with the auxiliary electrodes and another gel, run beside it. The dye front is slightly more curved for gels with auxiliary electrodes than for gels in the unmodified system (left panel). However, the neighboring gel shows a significant decrease in initial curvature and in change in curvature during the separation relative to behavior in the unmodified box. Both “frowns” and “smiles” are less for the dye in the unmodified system. The right panel shows similar behavior for the tilt or skewness. In the gel with auxiliary electrodes, there is no significant difference from the unmodified gels. However, in gels near the auxiliary electrodes, the skewing is almost eliminated, having both an initial value and a slope that are much closer to zero than those in unmodified gels. The conclusion drawn is that auxiliary electrodes offer the possibility of improved behavior but that placement is critical and not yet optimized. More generally, it is clear from these results that the potential gradients in the unmodified box are far from uniform.

6.2. Temperature variability

Next, attention is turned to possible temperature inequalities and the effectiveness of stirring to eliminate these. Visible tracers were put in the lower buffer and their motion was observed over time.

Fig. 9 shows the positions of a soluble dye pulse at various times after injection between the first and second gels in the electrophoresis box. The dye was injected in a line at the horizontal center of the gel and pictures were taken at the times indicated. Expected flow is horizontal from right to left across the face of the gel. However, observation shows some of the dye moves to the right and other portions even appear to circulate. Moreover, motion is surprisingly slow.

Fig. 10 shows the trajectories of neutrally buoyant oil drops in the stirred electrophoresis box. These oil drops can be seen to circulate in approximately the same region of the gel, rather than flowing steadily from right to left. Furthermore, they all follow slightly different paths, indicating that the flow varies with time.

It is now clear that buffer circulation is both very slow and far from the uniform right-to-left motion expected, and these observations are consistent with the formation of “smiles” as well as the spreading of current lines shown in Fig. 5. It remains to estimate the extent of these effects.

The heat transfer from the gels to the lower buffer is directly related to the velocity of the coolant. The dependence of the heat transfer coefficient on velocity for this system, which has simultaneously developing temperature and momentum boundary layers, can be found in the literature ([10], Eq. (5.214)). Since the cooling fluid in this system circulates, there will be stagnant points at the center of the circulating areas. Far from the areas of recirculation, the average velocity was measured to be ~ 1 cm/s. The change in heat transfer produced by these velocity variations will lead to varying temperatures at the center of the gel. Since ion mobilities change by $\sim 2.5\%/^{\circ}\text{C}$ [11], it is expected that the ions will

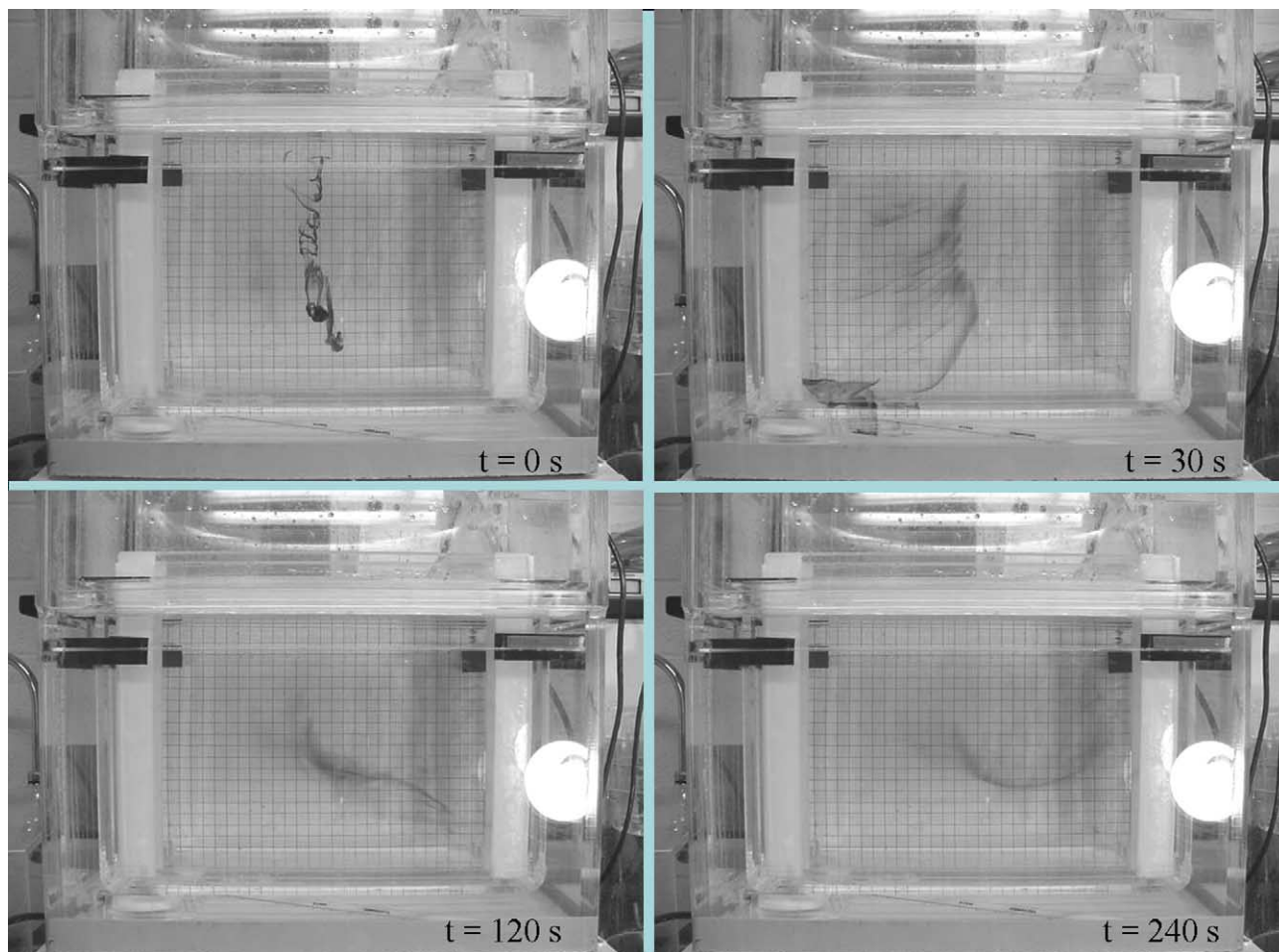


Fig. 9. Diagnosis of coolant flow patterns. Dye was injected between the first and second gels in the gel box, and pictures were taken at the times indicated.

move noticeably faster (as evidenced by the dye front) in areas where the cooling fluid is stagnant, producing curvature in the dye front. Additionally, the fluid, which flows from right to left across the face of the gel, warms up as it flows past the gel. Typically 16 W of power is dissipated in each

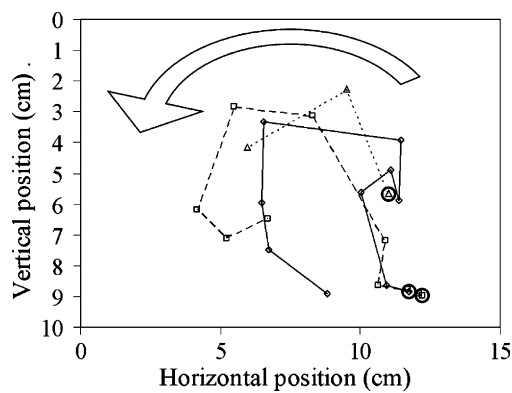


Fig. 10. Trajectories of three oil drops. The first point in each trajectory is circled. Oil drops were a neutrally buoyant mixture of dibutyl phthalate and heptane.

gel, with more heat being released behind the dye front where the voltage gradient is steeper. This heat is transferred to the surrounding buffer. The temperature change in the coolant depends on its velocity past the gel, which determines the volume of coolant that will absorb the heat. Because of the slow movement of the fluid past the gels, it is calculated that the cooling buffer will show approximately a 0.5 °C temperature rise by the time it reaches the left side of the gel, inducing skewing of the dye front.

Several tests were done to determine the extent to which temperature variations induced by flow variations produced curvature and skewing of the dye front. First, the stirring and cooling were turned off so that all the fluid was stagnant. This is expected to reduce the left to right skewing since no fluid is flowing across the face of the gel and becoming warmer. The results in the left panel of Fig. 11 support this hypothesis. Plots similar to those shown in Fig. 8 were developed for the unmodified system, the system with blocking and masking, and system with blocking and masking with no cooling or stirring. Since the temperature effects are time-variant but are not expected to be important for the initial curvature and skew, the change in curvature and skewing over time was found by

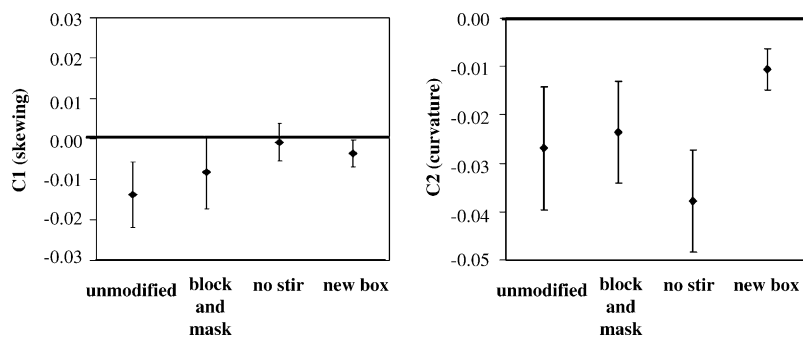


Fig. 11. Rate of change in curvature and skewing (represented by slopes of C_2 and C_1 vs. distance) for the original box, the original box with blocking and masking both with and without stirring, and the new box (including blocks, masking, and the honeycomb-patterned gel rack). Error bars show the standard deviation in the slope from a linear least squares fit to C_2 or C_1 vs. distance.

calculating the rate at which these coefficients changes with the distance traveled by the dye. This decoupled the initial shape of the dye front from its development over time. Fig. 11 shows that the changing skewing produced during the run is considerably less when the cooling and stirring are turned off. It also has a smaller standard deviation because it is more uniform from run to run. This indicates that the right to left flow across the gel is largely responsible for the observed skewing. Eliminating the right to left flow nearly eliminates the tilt of the dye front. The curvature, however, is larger in when the stirring is turned off, as shown in the right panel of Fig. 11, making it necessary to find an alternative that would allow the buffer to be cooled and stirred while reducing the effects of flow variations. Therefore, a new gel support rack was built with the aim of improving the uniformity of the coolant flow past the gels. It was designed with a honeycomb pattern of holes to allow the fluid to flow more rapidly past the gels and to decrease the local circulation of the cooling buffer. The skewing using this new rack was nearly as small as it was using the old rack without stirring in terms of both amount of skewing produced during the run and the gel-to-gel variation. Additionally, the curvature was improved over the other three configurations tested in terms of both the amount of curvature produced during the run and the gel-to-gel variation in the shape of the dye front. This indicates that some simple redesign to improve the uniformity of the coolant flow produces dramatic improvements in the reproducibility of ion migration both within a gel, by eliminating the left to right variations and variations due to stagnancy, and between gels by reducing positional and temporal flow variations.

7. Conclusions

Careful quantitative observation of carrier electrolyte dynamics suggests many causes for departures of observations from the simple rectilinear migration normally assumed for this widely used operation. The causes of these deviations include both operating conditions and equipment design. While SDS is a contributing factor, the deviations persist even in the absence of SDS. Other contributing factors include the

reservoir buffer compositions, which are not factored into the model. Departures from the one-dimensional migration assumed in the model are most likely the primary cause of remaining deviations. The curvature and skewing of the dye front can be used to study the extent of divergence of current paths in the gel. Both can be minimized by altering the current paths and improving the stirring of the cooling buffer. Blocking the extraneous parts of the buffer reservoir and masking the electrodes, or alternatively adding auxiliary electrodes, improved the shape of the dye front. Likewise, changing the configuration of the gel rack to minimize circulation and improve the flow uniformity and rate past the gels decreased the amount of curving and skewing.

Based on the observations in this study, recommendations can be made for operating conditions and equipment design changes that will improve the predictability of ion migration. It has been shown that recycling the bottom buffer leads to increased departures from the model and larger run-to-run variability. Therefore, it is recommended that fresh buffer be used for each electrophoresis run. This will improve the efficiency of the separation so that gels will finish more quickly using the same current. It will also improve the reproducibility of the separation process by eliminating variations caused by different starting buffer concentrations. Additionally, the box can be redesigned to ensure vertical current paths entering the gel and uniform temperature distribution across the face of the gel. These modifications should decrease the divergence of current lines, improving the predictability and reproducibility of ion migration.

Appendix A. Parameters needed for the model

A.1. Experimental

To predict the migration velocity of ions under electrophoretic conditions, their conductances in a gel at $\sim 5^\circ\text{C}$ are needed. First, the conductance was measured in solution at room temperature. Then, the conductance in the gel was measured at room temperature. Finally, the temperature dependence was found.

Conductances were measured using solutions in capillary tubes of known cross-sectional area. The capillary was placed through the side arms of two side-arm flasks, creating a bridge between them. The flasks were filled with buffer above the level of the capillary. Two electrodes were connected to a voltmeter, and one was placed in each end of the capillary. A power supply was connected to an ammeter, and one electrode was attached to each. One of these electrodes was placed in each of the buffer reservoirs (flasks). A voltage of 1–4 V was applied from the power supply. The voltage drop and current were measured over a capillary between two stirred reservoirs. Before each reading, a reading was taken at 0 V, and this value was subtracted from the reading at other settings. The 0 V reading was generally consistent for all measurements.

The electrodes used to measure the voltage and current were platinized 0.25 mm diameter annealed platinum wire. Platinization was carried out using the protocol outlined in *Metrohm Application Bulletin 64/2e*. The voltage (V) and current (I) are plotted to find the resistance in the capillary. They are related by Ohm's law, $V = IR$. For this geometry, the resistance is

$$R = \frac{L}{A \sum (c_i \lambda_i)} \quad (\text{A.1})$$

where L is the length of the capillary, A the cross-sectional area, c the concentration of each species, and λ the conductance with the i subscript indicating that the sum is over all species present.

Knowing the voltage, current, concentration, and geometry, the sum of the anion and cation conductances in the solution can be found. The unknown conductances were found by measuring their conductances in solutions with a counterion of known conductance. The chloride conductance was found from a 100 mM solution of potassium chloride. The Tris concentration was then found from a 123 mM solution of Tris–HCl (both with excess Tris, as used in the gels, and without excess Tris). The glycinate conductance was found from a solution of 16 mM glycine with 16 mM KOH.

The same apparatus was also used to find the conductance of ions in the gel matrix. Gels were cast in capillary tubes, and the Tris buffer in the gel recipe (see Section 2) was replaced by the solution to be analyzed. The flasks were filled with a solution of the same buffer at the same concentrations as that used in the gel. Conductances were found in the same way as for the ions in solution. The buffers used in the gels were at the same concentrations as those in solution so that direct comparisons could be made (100 mM potassium chloride, 123 mM Tris–HCl, and 16 mM glycine with 16 mM KOH).

Next, the temperature dependence was measured by finding the conductivity of solutions in a beaker. The conductance was calculated by the equation

$$\Lambda = \sum c_i \lambda_i \quad (\text{A.2})$$

where Λ is the conductivity of the solution. For cold measurements, the beaker was placed in a stirred ice bath and for hot measurements it was in a stirred boiling water bath. The Fischer Scientific Digital Conductivity Meter gave both the conductivity and the temperature of the solution. Readings were taken 2 min after the probe was placed in the solution. This was sufficient time for the room temperature solution to give a steady reading. The meter automatically corrected for temperature by 2% for each degree different from 25 °C. Therefore, the following adjustment was made to the meter output to find the actual conductivity of the solution.

$$\Lambda = \Lambda_{\text{measured}} e^{0.02(T-25)} \quad (\text{A.3})$$

The conductance of either the anion or the cation can be found by measuring its conductivity in solution with a counterion of known conductance. The chloride conductance was found from a 6.78 mM solution of potassium chloride. Tris was found from a solution of 39 mM Tris base with 16 mM Tris–HCl. Glycinate conductance was found from a solution of 99.6 mM Tris base with 160 mM glycine. Concentrations were chosen to stay within the range of the conductivity meter.

A.2. Results

Several parameters are needed in the model to calculate the position of the dye front. The dissociation constants for Tris and glycine are needed to find ion concentrations. The conductances of all the ions present in the gels and buffers are necessary to find their mobilities.

Since the potential drop will only affect ions and not undissociated molecules, the concentration of dissociated molecules is important for the model. Tris–HCl is assumed to be completely dissociated. Both Tris and glycinate pK 's as a function of temperature are available in the literature [12]; therefore, no measurements were necessary for dissociation constants. Fits to the literature data gave the following temperature dependencies over the range of interest:

$$pK_{\text{Tris}} = (-0.027 \pm 0.0008)T + (8.77 \pm 0.03), \quad (6 \text{ points}) \quad (\text{A.4})$$

$$pK_{\text{glycine}} = -0.021T + 10.31, \quad (2 \text{ points}) \quad (\text{A.5})$$

Conductances of the Tris and glycinate ions had to be measured. The conductance of chloride is available in the literature [11]. The first step to determining the conductances of ions is to find the conductance in solution at room temperature. Using the capillary apparatus described above, the voltage and current were recorded and plotted. In most cases, there is only one cation and one anion in the solution, so the concentration can be factored out of the sum in Eq. (A.1), and the sum of the conductances can be found. The sum of the conductances of potassium and chloride at 25 °C is given in the literature to be 128 S cm²/eq. [11]. Measured conductivity at the same concentration (100 mM) is

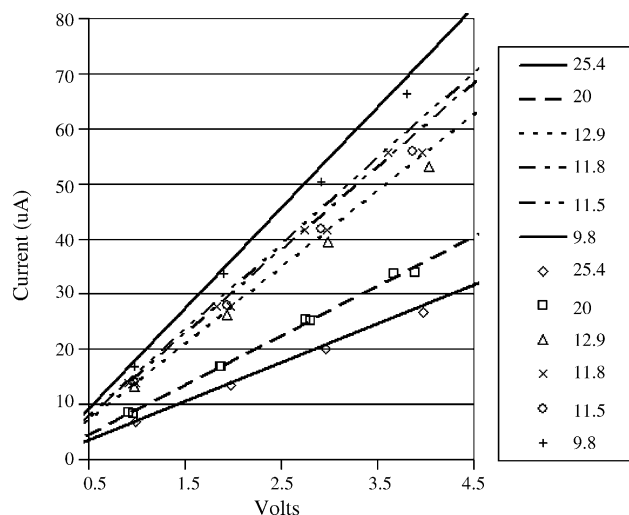


Fig. A.1. Theoretical voltage vs. current relationships for capillaries of various lengths in centimeters. The lines represent literature values [11], and the points represent measured values.

122 S cm²/eq., which is less than 5% different from the literature value.

Fig. A.1 shows a plot of voltage versus current from the capillary apparatus. The lines in this figure represent predictions based on the literature values of KCl conductivity [11]. The points represent measured values. In Fig. A.1, the predictions (lines) are seen to agree well with the measured values (points), especially for the longest capillaries. As a result, only capillaries longer than 25 cm were used for the following calculations.

Conductances of individual ions were found from the conductivity, which is the reciprocal of the resistance, given in Eq. (A.1). It was assumed that the ratio of potassium conductance to chloride conductance was the same as the reported values at infinite dilution. This gave a chloride conductance of 66.33 S cm²/eq. The measured chloride conductance was used to calculate a Tris conductance of 13.17 S cm²/eq. The potassium and hydroxide conductances found in the litera-

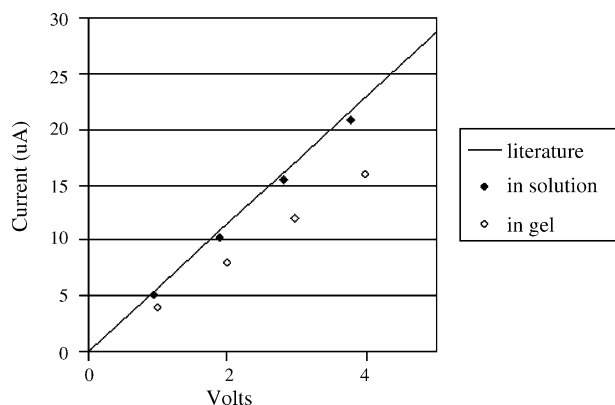


Fig. A.2. Comparison of literature resistance to measured resistance in solution and in gels. The line is based on literature values [11]. The closed diamonds represent the measured solution values and agree well with the literature. The open diamonds represent the measured gel values.

ture [11] were used to calculate a glycine conductance of 35.3 S cm²/eq. These results are summarized in Table A.1.

Fig. A.2 shows the current versus voltage plot for potassium chloride in solution (closed diamonds) and in gels (open diamonds). These measurements are compared to the literature values [11], shown by the solid line. The measured conductivity, which is the slope of a straight line fit to the data, agrees within 4% with the literature values. The conductivity in the gel (0.009 S/cm) is about 72% of that in solution (0.012 S/cm), as evidenced by the smaller slope of a straight line fit to the current as a function of voltage. This gave a chloride conductance of 44.95 S cm²/eq. in the gel, assuming the same ratio of potassium to chloride conductance as in solution. The conductivity of Tris–HCl was 0.006 S/cm in the gel, as opposed to 0.009 S/cm in solution. The gel value was approximately 60% of the solution value, which seems reasonable based on the KCl results. However, when the Tris conductance was found using a chloride conductance of 44.95 S cm²/eq., it was about 0.15 S cm²/eq., only 1.1% of its solution value of 13.17 S cm²/eq. This highly unexpected

Table A.1
Measured conductances of chloride, Tris, and glycinate in solution and gels

	$\lambda_K + \lambda_{Cl}$ (S cm ² /eq.)	Ratio (gels/solutions)	λ_K (S cm ² /eq.)	λ_{Cl} (S cm ² /eq.)	
KCl					
Robinson and Stokes	129.00		Assume ratio is the same as in the limiting case		
Solution	122.22		59.89	62.33	
Gels	88.14	0.72	43.19	44.95	Cl gel/solution 0.72
	$\lambda_{Tris} + \lambda_{Cl}$ (S cm ² /eq.)		λ_T (S cm ² /eq.)	λ_{Cl} (S cm ² /eq.)	
Tris–HCl					
Solution	75.50		13.17	62.33	
Gels	45.10	0.60	0.15	44.95	Tris gel/solution 0.01
	$\sum(c_i \lambda_i)$		λ_K (S cm ² /eq.)	λ_{OH} (S cm ² /eq.)	λ_G (S cm ² /eq.)
Glycine KOH					
Solution	1522.46		59.89	198.30	35.27
Gels	1366.05	0.90	43.19	144.76	42.19
					Glycine gel/solution 1.20

result indicates that there are other factors, such as interactions of ions with the matrix, affecting the conductivity measurements in the gel. An equally unexpected result was found for glycinate, which had a measured conductance in the gel (42.2 S cm²/eq.) that was 20% higher than its solution value (35.3 S cm²/eq.).

Table A.1 summarizes the conductance measurements from the capillary apparatus. The first column gives the sum of the ion conductances for the systems in which there were only two ions of equal concentration. For the glycinate measurements, in which three ions at unequal concentrations were present, the sum of the concentration × conductivity product is given. For KCl, it was assumed that the ratio of potassium to chloride conductance in dilute solution was the same as the ratio at infinite dilution [11]. The calculated potassium and chloride conductances were used to find the Tris and glycinate conductances. The hydroxide conductance was found in the literature [11]. The infinite dilution value was used, but the concentration is low enough that slight differences should not significantly affect the calculated glycinate conductance. The last column gives the ratio of conductances in gels and solutions, which in some cases is very different from the conductivity ratios in the second column.

The unusual relationship between solution and gel conductances for Tris and glycinate are not well understood. Therefore, in all cases 72% of the conductance in solution was used as the gel conductance, based on the potassium chloride measurements. The room temperature conductances used were 44.95 S cm²/eq. for chloride, 9.5 S cm²/eq. for Tris, and 25.4 S cm²/eq. for glycinate.

After finding the room temperature conductances, the temperature dependence needed to be determined. Fig. A.3 shows the temperature dependence of the conductance for chloride, including an exponential fit to the data. Literature values [11], which are shown by the dotted line, are also included for comparison. The temperature dependence of Tris and glycinate were found similarly; however, no literature values were

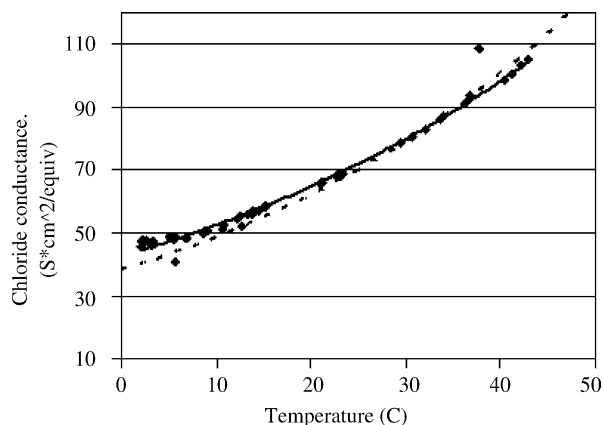


Fig. A.3. Conductivity as a function of temperature for chloride anions in a 6.8 mM solution of potassium chloride. The temperature dependence reported in the literature for ions at infinite dilution [11] is shown as a dashed line.

available for comparison. The conductances are given by

$$\lambda_{\text{Cl}^-} = (42.62 \pm 0.03)e^{(0.021 \pm 0.0004)T} \quad (\text{A.6})$$

$$\lambda_{\text{T}^+} = (11.11 \pm 0.12)e^{(0.031 \pm 0.003)T} \quad (\text{A.7})$$

$$\lambda_{\text{G}^-} = (18.87 \pm 0.09)e^{(0.028 \pm 0.001)T} \quad (\text{A.8})$$

The slope of the temperature dependence (given by the coefficient of T in the exponential) was used to calculate the conductance in the model as a function of temperature. The more reliable capillary measurements were used to find the conductance at $T=0$ in the gel. The following relationships were used to estimate the ion conductances in the model:

$$\lambda_{\text{Cl}^-} = (29.59 \pm 0.19)e^{(0.021 \pm 0.0004)T} \quad (\text{A.9})$$

$$\lambda_{\text{T}^+} = (5.15 \pm 0.35)e^{(0.031 \pm 0.003)T} \quad (\text{A.10})$$

$$\lambda_{\text{G}^-} = (14.57 \pm 0.39)e^{(0.028 \pm 0.001)T} \quad (\text{A.11})$$

Appendix B. Development of the current-based model

Current, which is measured during electrophoresis, can be used to find the velocity with which ions move through the gel. Current is continuous throughout the system; therefore, the current in the upper and lower parts of the gel can be equated.

$$I_i = AF \left(\sum N_i \right) \quad (\text{B.1})$$

$$N_i = c_i v_i = c_i \frac{\lambda_i \nabla \phi}{F} \quad (\text{B.2})$$

$$I_L = I_U \quad (\text{B.3})$$

where I is the current in either the upper (U) or lower (L) part of the gel, A the cross-sectional area, F Faraday's constant, c_i the concentration, v_i the velocity, and N_i the molar flux of species i . Putting Eq. (B.1) into Eq. (B.2), the following relationship between current and velocity is obtained.

$$\begin{aligned} I &= AF(c_{\text{Cl}^-} v_{\text{Cl}^-} - c_{\text{T}^+,L} v_{\text{T}^+,L}) \\ &= AF(c_{\text{G}^-} v_{\text{G}^-} - c_{\text{T}^+,U} v_{\text{T}^+,U}) \end{aligned} \quad (\text{B.4})$$

The subscripts are defined as follows: Cl⁻ chloride; T⁺,L Tris in the lower part of the gel; G⁻ glycinate; and T⁺,U Tris in the upper portion of the gel. Because of electroneutrality, the lower Tris concentration is equal to the chloride concentration and the upper Tris concentration is equal to the glycinate concentration.

$$I = AFc_{\text{Cl}^-}(v_{\text{Cl}^-} - v_{\text{T}^+,L}) = AFc_{\text{G}^-}(v_{\text{G}^-} - v_{\text{T}^+,U}) \quad (\text{B.5})$$

The velocity of each ion is determined by its mobility and the driving force for migration, which in this case is the potential drop in each portion of the gel.

$$v_{\text{Cl}^-} = \frac{\lambda_{\text{Cl}^-} \nabla \phi_L}{F} \quad (\text{B.6})$$

$$v_{T^+,L} = \frac{\lambda_{T^+} \nabla \phi_L}{F} \quad (\text{B.7})$$

Solving these equations for the potential drop and setting them equal, a relationship between the Tris and chloride velocities is obtained.

$$v_{T^+,L} = - \left(\frac{\lambda_{T^+}}{\lambda_{Cl^-}} \right) v_{Cl^-} \quad (\text{B.8})$$

Using a similar strategy for the upper part of the gel, the Tris velocity is expressed in terms of the glycinate velocity.

$$v_{T^+,U} = - \left(\frac{\lambda_{T^+}}{\lambda_{G^-}} \right) v_{G^-} \quad (\text{B.9})$$

Inserting these expressions into Eq. (B.4) gives a relationship between current and velocity in terms of known quantities.

$$\begin{aligned} I &= AFc_{Cl^-} \left(1 + \frac{\lambda_{T^+,L}}{\lambda_{Cl^-}} \right) v_{Cl^-} \\ &= AFc_{G^-} \left(1 + \frac{\lambda_{T^+,U}}{\lambda_{G^-}} \right) v_{G^-} \end{aligned} \quad (\text{B.10})$$

The chloride and glycinate both travel at the velocity of the interface because of Kohlraush stacking, so this equation gives two expressions for the interface velocity.

$$\begin{aligned} v_{\text{interface}} &= \frac{I}{AFc_{Cl^-} (1 + (\lambda_{T^+,L}/\lambda_{Cl^-}))} \\ &= \frac{I}{AFc_{G^-} (1 + (\lambda_{T^+,U}/\lambda_{G^-}))} \end{aligned} \quad (\text{B.11})$$

The chloride expression is more straightforward because Tris–HCl is completely dissociated, making the ionized chloride concentration easy to calculate. Therefore, that expression will be used to predict the distance traveled by the interface. However, the glycinate concentration was calculated from the stacking velocity and dissociation equilibria, and

the velocity values agree for the two expressions for all data sets.

The distance traveled by the interface is found by integrating Eq. (B.11) with respect to time.

$$\int_0^x v_{\text{interface}} dt = \frac{1}{AFc_{Cl^-} (1 + (\lambda_{T^+,L}/\lambda_{Cl^-}))} \int_0^Q I dt \quad (\text{B.12})$$

Q is the number of coulombs of current passed through the system when the dye front has traveled a distance x . Performing the integral gives the final expression for the distance traveled by the tracer dye.

$$x = \frac{Q}{AFc_{Cl^-} (1 + (\lambda_{T^+,L}/\lambda_{Cl^-}))} \quad (\text{B.13})$$

References

- [1] P. O'Farrell, *J. Biol. Chem.* 250 (1975) 4007.
- [2] E. Gianazza, S. Astrua-Testori, P. Caccia, P. Giacon, L. Quaglia, P.G. Righetti, *Electrophoresis* 7 (1986) 76.
- [3] T. Voss, P. Haberl, *Electrophoresis* 21 (2000) 3345.
- [4] F. Kohlraush, *Ann. Phys. Chem.* 10 (1897) 209.
- [5] E.B. Dismukes, R.A. Alberty, *J. Am. Chem. Soc.* 76 (1954) 191.
- [6] L. Ornstein, in: H.E. Whipple (Ed.), *Gel Electrophoresis*, The New York Academy of Sciences, New York, 1964, p. 321.
- [7] W.M. Deen, *Analysis of Transport Phenomena*, Oxford University Press, New York, 1998.
- [8] R.B. Bird, W.E. Stewart, E.N. Lightfoot, *Transport Phenomena*, Wiley, Inc., New York, 2002.
- [9] M. Wyckoff, D. Rodbard, A. Chrambach, *Anal. Biochem.* 78 (1976) 459.
- [10] W.M. Rohsenow, J.P. Hartnett, Y.I. Cho, *Handbook of Heat Transfer*, McGraw-Hill, New York, 1998.
- [11] R. Robinson, R. Stokes, *Electrolyte Solutions*, Butterworths, London, 1959.
- [12] R.M. Izatt, J.J. Christensen, in: H.A. Sober (Ed.), *Handbook of Biochemistry*, CRC Press, Cleveland, OH, 1970, p. J58.